MD-Vol. 9

NEW DIRECTIONS IN THE NONDESTRUCTIVE EVALUATION OF ADVANCED MATERIALS

edited by
J. L. ROSE
A. A. TSENG

MD-Vol. 9

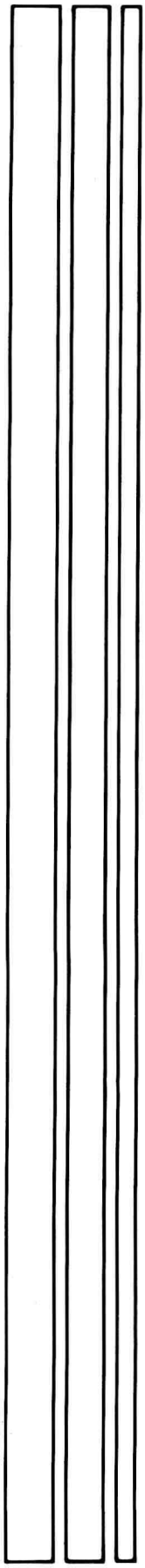

NEW DIRECTIONS IN THE NONDESTRUCTIVE EVALUATION OF ADVANCED MATERIALS

presented at

THE WINTER ANNUAL MEETING OF
THE AMERICAN SOCIETY OF MECHANICAL ENGINEERS
CHICAGO, ILLINOIS
NOVEMBER 27–DECEMBER 2, 1988

sponsored by

THE MATERIALS DIVISION, ASME

edited by

J. L. ROSE
DREXEL UNIVERSITY

A. A. TSENG
DREXEL UNIVERSITY

THE AMERICAN SOCIETY OF MECHANICAL ENGINEERS
United Engineering Center 345 East 47th Street New York, N.Y. 10017

Library of Congress Catalog Number 88-82836

FOREWORD

Nondestructive Evaluation Engineering has grown steadily for the past twenty years, going through a transition phase from an art to a multi-disciplinary area of study in science and engineering. An increased awareness of the benefits of NDE in safety and cost savings has come about in industry, government and university. Over fifty universities offer graduate course work and advanced thesis topics on subjects of NDE compared to just two key universities twenty years ago. Expenditures in research, manufacturing quality control, and in in-service inspection have increased rapidly over the past decade. The forecast for NDE utilization in the future is even stronger with emphasis being directed towards on-line monitoring in manufacturing, and also on new inspection techniques for such advanced materials as ceramics and composite materials.

Assembled in this symposium volume are contributions from the world's leading experts on some new directions in nondestructive evaluation. Finite element modeling possibilities of wave propagation are reviewed for assistance in ultrasonic NDE. Aspects of mode conversion, neutron diffraction NDE principles for advanced composites, and ceramic inspection guidelines from ultrasonics, micro-radiography, and tomography are covered. For composite materials, such topics as ultrasonic velocity measurements for quantitative NDE, acoustographic NDE, current accept/reject criteria, and ultrasonic imaging enhancement techniques are discussed. The concept of a feature matrix based on anisotropic elasticity is introduced as a new consideration in ultrasonic NDE. Surface wave considerations are outlined. In addition, a variety of physical models are presented that will become useful in the near future in data collection methodology and analysis for advanced materials. Wave reflection from a crack permeated diffusion bond and also from an adhesive bond are included along with ultrasonic scattering analysis from intergranular stress corrosion cracking. Elastic guided wave analysis is also presented along with displacement and stress distribution analysis in a plate for improved sensitivity in NDE.

In summary, the new directions in the nondestructive evaluation of advanced materials are illustrated quite well in this symposium volume. New concepts are being introduced on a regular basis with an ever-increasing number of users and participants in the NDE research and development community.

The editors would like to thank the contributors to this volume for their efforts in preparing this excellent manuscript under the imposed time constraints. Special thanks go to Mrs. Jadwiga Pilarski and Renee Erdman for their coordination efforts throughout the preparation for this symposium and the bound volume.

Joseph L. Rose
Ampere A. Tseng
Department of Mechanical Engineering and Mechanics
Drexel University

CONTENTS

FINITE ELEMENT MODELING OF ULTRASONIC WAVE PROPAGATION IN MATERIALS

W. Lord
Electrical Engineering Department
Colorado State University
Fort Collins, Colorado

R. Ludwig
Electrical Engineering Department
Worcester Polytechnic Institute
Worcester, Massachusetts

Z. You
Electrical Engineering Department
Colorado State University
Fort Collins, Colorado

ABSTRACT

Ultrasonic interrogation of advanced materials for defects and the measurement of material properties is hampered by the lack of a viable model capable of predicting the realistic transducer signals arising from complex ultrasound/material interactions.

This paper describes the application of a finite element model to this problem and gives results showing how the finite element code can be used to predict wave propagation phenomena. Both isotropic and anisotropic materials have been simulated this way and the results clearly show the potential of this numerical model to aid in the solution of forward and inverse problems associated with the ultrasonic inspection of materials.

NOMENCLATURE

C_L = compressional wave velocity, in/sec.

C_S = shear wave velocity, in/sec.

F = energy functional, ft-lb.

$\{F\}$ = surface traction vector, lb/in^2.

$[K]$ = stiffness matrix, lb/in^2.

$[M]$ = mass matrix, lb.

$\underline{u}$ = displacement vector, in.

$\ddot{\underline{u}}$ = acceleration, in/sec^2.

$\underline{\underline{S}}$ = strain tensor

$\underline{\underline{T}}$ = stress tensor, lb/in^2.

$w(y)$ = weighting function, in.

t = time, sec.

$\hat{\underline{z}}$ = unit vector in z-direction.

δ = first variation, delta function.

∇ = del operator.

ρ = material density, lb.

$\omega_o = 2\pi f_o$ = angular frequency, 1/sec.

$\theta(y)$ = phase delay, sec.

$\underline{\tau}$ = traction, lb/in^2.

INTRODUCTION

All energy/defect interactions associated with the nondestructive evaluation (NDE) of materials are describable by some form of partial differential equation (PDE). For example, electrostatic and magnetostatic methods such as potential drop, magnetic particle, magnetography and flux leakage NDE methods are governed by elliptic equations of Laplace's or Poisson's form; all eddy current NDE methods including single frequency, multi-frequency and pulsed techniques are governed by a parabolic diffusion equation, and finally microwave and ultrasonic methods of defect detection are governed by hyperbolic wave equations.

This wide variety of inspection mechanisms (for the sake of brevity not all have been included in this brief introduction) which constitute the science of nondestructive evaluation, together with their corresponding mathematical description contribute to most of the richness and challenge associated with the modeling of NDE phenomena. This is particularly true when one considers the host material properties which are often nonlinear, NDE test geometries and realistic defect shapes, all of which have to be incorporated into the appropriate PDE solution algorithm. From an analytical standpoint, the inclusion of such severe constraints in the definition of either the forward problem (given an input transducer signal and a specific defect shape, what is the output transducer signal) or the inverse problem (given the input and output transducer signals, what is the shape and location of the material defect), leads to the use of idealized sources, test geometries and defect shapes, thus limiting the application range of any derived results.

Fortunately, the urgent need to model NDE energy/defect interactions has occurred at a time of increasing computational capability associated with modern computers, and the concomitant development of powerful numerical PDE solution strategies such as finite difference, boundary elements, and finite element algorithms. The finite element technique has in fact been applied sequentially over the past twenty years by the author's research group to the solution of the elliptic, parabolic and, most recently, hyperbolic PDE's associated with electromagnetic and ultrasonic NDE forms. Starting with the simplest of two dimensional (2-D) elliptic, magnetostatic leakage field problems (Hwang and Lord, 1975), the numerical code has subsequently been extended to axisymmetric (Palanisamy and Lord, 1980a) and three dimensional (3-D) geometries (Ida and Lord, 1983). Similar development has taken place in the case of parabolic eddy current NDE modeling as computer power has steadily mounted over the years. Again, starting with simple 2-D geometries (Palanisamy and Lord, 1980b), the eddy current code has been extended to axisymmetric (Lord and Palanisamy, 1981) and 3-D geometries (Ida and Lord, 1985), although it should be noted that for single frequency eddy current NDE, the governing parabolic PDE reduces to an elliptic form upon the substitution of $j\omega$ for d/dt. Pulsed eddy current methods have to date only been studied for 2-D geometries (Allen and Lord, 1984) because of the need for both space and time discretization. The use of finite element analysis techniques for modeling low frequency electromagnetic NDE phenomena provides a unified approach to the subject (Lord, 1983 and 1987), and shows how numerical code cannot only be used for examining the physics of field/specimen interactions (Lord, et al., 1983), but also provides a useful design tool (Ida et al., 1983), an experimental test rig (Ida et al., 1985) and a technique for validating NDE signal processing schemes (Udpa and Lord, 1984).

In carrying out the 3-D eddy current NDE studies (Ida and Lord, 1985), use had to be made of the vector processing capabilities of modern supercomputers, and it was realized that such computational power ought to allow solution of the hyperbolic wave equations governing ultrasonic NDE phenomena. Consequently, a simple 2-D formulation was developed and applied to the study of wave propagation and scattering in an aluminum block (Ludwig and Lord, 1988a). This paper gives results of additional finite element work extending the modeling to wave interactions with tight cracks, anisotropic materials and surface waves.

THEORETICAL CONSIDERATIONS

The initial application of finite element code to the study of a magnetostatic leakage fields around defects in ferromagnetic materials occurred at a time when considerable disagreement existed in the scientific community as to the relative merits of finite difference and finite element methods of analysis (see, for example, Silvester and Chari, 1970; Demerdash and Nehl, 1970). A finite element formulation of the problem was chosen because of the peculiar constraints associated with NDE phenomena modeling, namely awkward defect shapes, nonlinear material properties, complex boundary conditions associated with practical test geometries and the need to extend the modeling to three-dimensions. As many of the first code applications involved tubing geometries having symmetry about the tube axis, it was possible to take advantage of an axisymmetric formulation giving exact results directly comparable with experimental measurements (Lord et al. 1983). In addition, the modeling was aided by the fact that the fields were well behaved, in the sense that they were confined to a relatively small area around the excitation source, and the probe excitation levels were so low that initial permeability values could be used to characterize the ferromagnetic material. These points are mentioned in order to provide a contrast with the wave propagation modeling problems associated with ultrasonic NDE. Although finite difference formulations have been used to study ultrasonic wave propagation (Harumi et al., 1973 and Bond, 1982) our experience with low frequency electromagnetic NDE modeling led us to believe that a finite element formulation could be developed, capable of modeling 2-D linear and non-linear ultrasonic NDE phenomena with possible extension to 3-D.

The finite element approach (Zienkiewicz, 1977; Bathe, 1982), rather than solving the governing hyperbolic PDE

$$C_L^2 \nabla^2 \underline{u} - c_s^2 \nabla \times \nabla \times \underline{u} - \frac{\partial^2 \underline{u}}{\partial t^2} = 0 \qquad (1)$$

directly, seeks to minimize the energy related functional F by differentiation

$$\frac{\delta F}{\delta u_i} = \frac{\delta}{\delta u_i} \left\{ \frac{1}{2} \int_v S:T dv + \int_v \underline{u} \cdot \frac{\delta^2 \underline{u}}{\delta t^2} \rho dv - \int_s \underline{u} \cdot \underline{\tau} ds \right\} \qquad (2)$$

This is done over a discretized region of interest where the nodal displacement values u are the unknowns and specific shape functions relate the displacement values at adjacent nodes. Introducing appropriate boundary conditions and carrying out the minimization indicated in equation (2) results in a matrix equation

$$[K] \{u\} + [M] \{\ddot{u}\} = \{F\} \qquad (3)$$

where the K and M matrices are related to the specific finite element shape functions chosen and the material properties expressed in terms of the shear and longitudinal velocities C_s and C_L of equation (1). In essence, equation (3) can be likened to a mass spring system in which the collection of all elements into the global matrix form represents the solid as an arrangement of masses interconnected to one another by springs. With an appropriate implicit time integration scheme, equation (3) can be solved by direct matrix inversion at each time step to yield unknown nodal displacements throughout the solution region which satisfy the governing hyperbolic equation (1). Code input requirements then relate to mesh geometry (including transducer aperture) material properties, boundary conditions and the digitized transducer waveform. Lacking a full-blown finite element representation of a piezoelectric transducer, the modeling studies to date have made use of digitized signals received from a through-transmission test on an unflawed aluminum block functioning as a calibration standard or, alternatively, the analytical approximation

$$f(t) = \left(1 - \cos \frac{\omega_o}{3} t\right) \cos \omega_o t \quad \text{for} \quad 0 \le t \le \frac{3\pi}{\omega_o} \qquad (4)$$

where $\omega_o = 2\pi f_o$ and f_o is the center frequency of the transducer. Either the experimentally determined transducer signal or the analytical function (4) can then be used to denote a two-dimensional displacement vector

$$\underline{u}(z,y,t) = \delta(z) w(y) f(t - \theta(y)) \hat{z} \qquad (5)$$

which serves as the forcing function in the global matrix equation (3). The function $\delta(z)$ (see Figure 1) ensures that the input displacement vector is only applied at the surface ($z=0$) of the specimen. $w(y)$ is a weighting function which allows any desired amplitude distribution of the applied transducer displacement over the finite aperture in the y direction and $\theta(y)$ allows the

transducer signal f(t) to be delayed over the transducer aperture, thus simulating the beam sterring behavior of an angle beam transducer (Ludwig et al., 1987). Unlike the low frequency electromagnetic NDE finite element code, advantage could not be taken of axisymmetry due to the limited practical application of such a formulation, consequently, care has had to be taken in validating the code. Experimental observations mode with a 1 MHz transducer in a through-transmission made on on aluminum block (Ludwig and Lord, 1988b) show good qualitative agreement with the corresponding finite element predictions and confirm that the code inherently models beam spread, mode conversion, and can accommodate pulsed transducer signals as well as arbitrarily shaped defects.

Neglecting the third dimension in ultrasonic NDE however, has considerably more significance than a similar assumption concerning low frequency NDE methods, and one should not expect experimental results from a 3-D world to agree exactly with the predictions from a 2-D model. For this reason additional comparison of the finite element code has been made with the analytically based Cagniard-deHoop formulation (Achenbach, 1973) for an infinite line source acting on a half-space. Results of this study (Ludwig et al, 1989) show excellent qualitative and quantitative agreement and provided the impetus needed for the study of anisotropic material effects and surface wave phenomena described in the following results section.

RESULTS

In order to illustrate the use of the finite element code to study the physical nature of ultrasound/material interactions, this paper considers the cases of a) surface waves generated by a point force source interacting with a tight surface breaking crack, b) bulk waves generated by the same source interacting with a tight interior crack, and c) waves from a finite aperture transducer interacting with an anistropic medium.

Surface Waves

Figure 1 shows the finite element code predictions for the first case of point source waves interacting with a surface breaking crack in an 8" x 4" (.2032 m x .1016m) aluminum block. Only 1/8 of the total block area is shown in the z-y plane and only the z displacements are plotted. The point force has the form of equation (4) and acts at t=0 at the center of the block on the z-x plane. In Figure 1a) the longitudinal wave has reached the 1/4" (.0064m) surface breaking tight crack and the surface and shear waves can be seen approaching the crack. At 10 microseconds (Figure 1b) the longitudinal wave is passing out of the viewing area, and the shear and surface waves are now interacting with the crack and being reflected by it. Figure 1c) after 14 microseconds shows the shear wave front past the crack, one component of the surface wave being reflected back from the crack and a second component propagating down the tight crack into the aluminum block. Finally at t=16 microseconds in Figure 1d) it can be seen that the tight crack has launched a wave traveling at the shear velocity into the aluminium block behind the original shear wave front.

Subsurface Crack

Figures 2a) through 2d) shows a similar progression for sound waves from a point force source interacting with the same tight crack (note that 1/2 the block is shown in this figure) at the center of an aluminum block. Longitudinal, shear, head and surface wave components can clearly be identified at all four time steps. Of particular interest is the reflected longitudinal wave shown at its origin in Figure 2b) and arriving at the front surface of the block in Figure 2d). The circular waves shown emanating from the tight crack in Figures 2c) and d) appear to be traveling at the shear wave velocity.

Anisotropy

Figure 3 shows a sequence of time steps for wave propagation in an anisotropic medium having the same elastic constants as uranium. The longitudinal, shear and surface waves can be seen emanating from a 1MHZ, 1/2" (.0127m) aperture transducer and propagating through and around the 4" x 4" (.1016m) block whose grain axis is parallel to the direction of propagation (z-axis). For the sake of brevity only the z displacements are shown. Of particular note, in contrast to Figures 4 and 5, is the focusing effect on the longitudinal wavefront of the grain structure parallel to the direction of propagation.

Figures 4 and 5 respectively show the defocussing and skewing effects of wave propagation perpendicular and at angle of 45° to the grain orientation of the orthorhombic material.

CONCLUSIONS

Modeling of energy/material interactions is a crucial step in the understanding and development of nondestructive evaluation techniques. Such models play a significant role in our physical knowledge of the phenomena as well as serving as useful design, simulation and calibration tools. Because of the unique constraints that practical NDE applications impose on the underlying PDE types, numerical methods such as finite element analysis are natural modeling choices particularly at a time when the computational power of modern computers is increasing rapidly. This paper discusses the development of a 2-D finite element model which is capable of predicting ultrasonic wave propagation modes in a variety of practical situations of interest to the NDE community. Although a full 3-D treatment will be needed in order to complete the modeling procedures the growing availability of parallel architecture computers such as the hypercube and transputer bodes well for the future.

ACKNOWLEDGMENTS

The authors are grateful to the Electric Power Research Institute for their support of this work under research project RP2687-2, Mike Avioli project manager. They would also like to acknowledge the contributions of Doug Moore at Worcester Polytechnic Institute and Mark Lusk at Colorado State University.

REFERENCES

Achenbach, J.D., 1973, Wave Propagation in Elastic Solids, North Holland.

Allen, B., and Lord, W., 1984, "Finite Element Modeling of Pulsed Eddy Current Phenomena", in Review of Progress in Quantitative Nondestructive Evaluation, Vol. 3, D.O. Thompson and D.E. Chimenti, Eds., Plenum, pp. 561-568.

Bathe, K.J., 1982, Finite Element Procedures in Engineering, Prentice Hall.

Bond, L.J., 1982, "Methods for the Computer Modelling of Ultrasonic Waves in Solids," in Research Techniques in Nondestructive Testing, Vol. 6, Ed. R.S. Sharpe, Academic Press, p. 107.

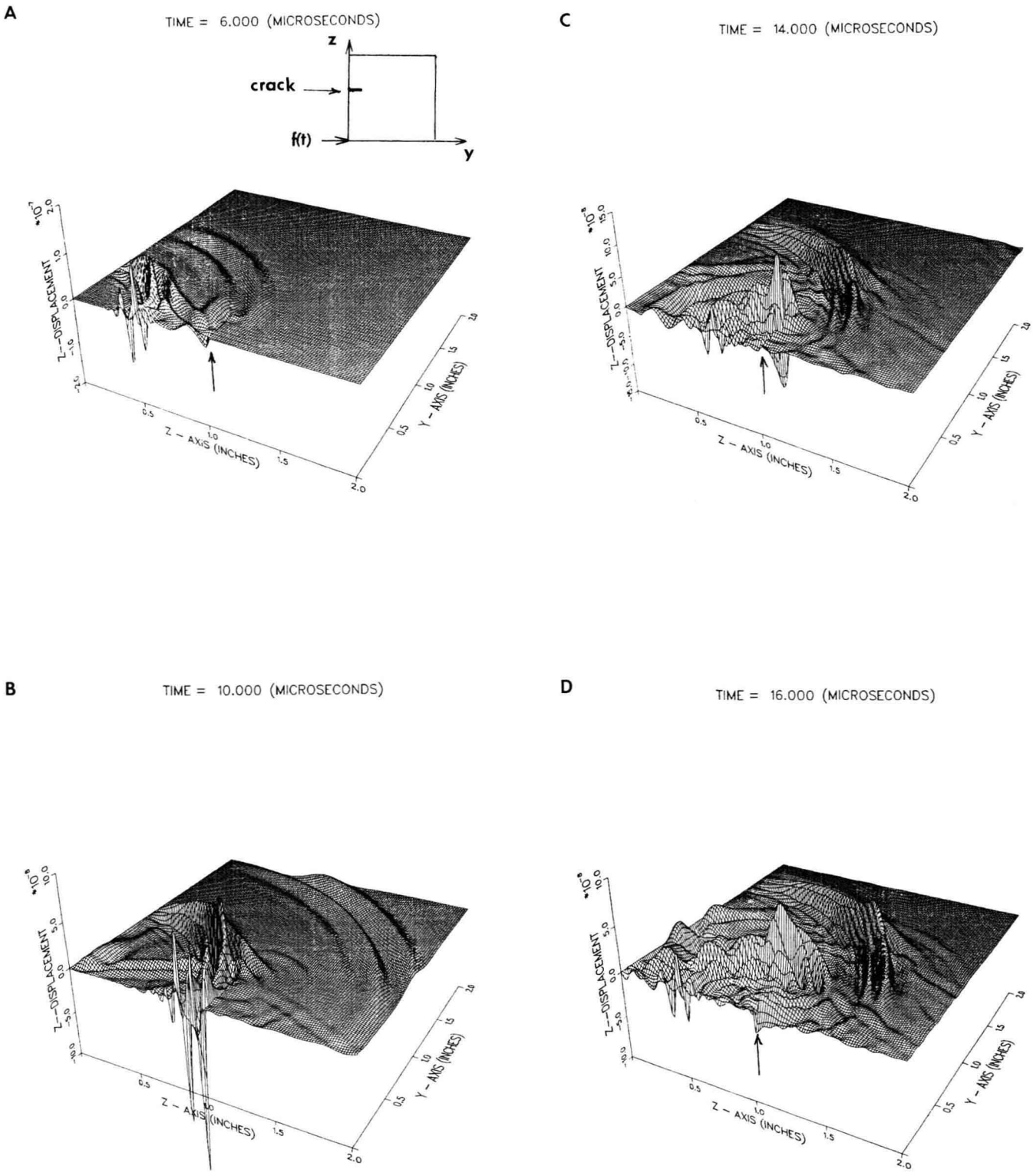

Fig. 1. Surface wave interactions with a tight surface breaking crack in an aluminum block.

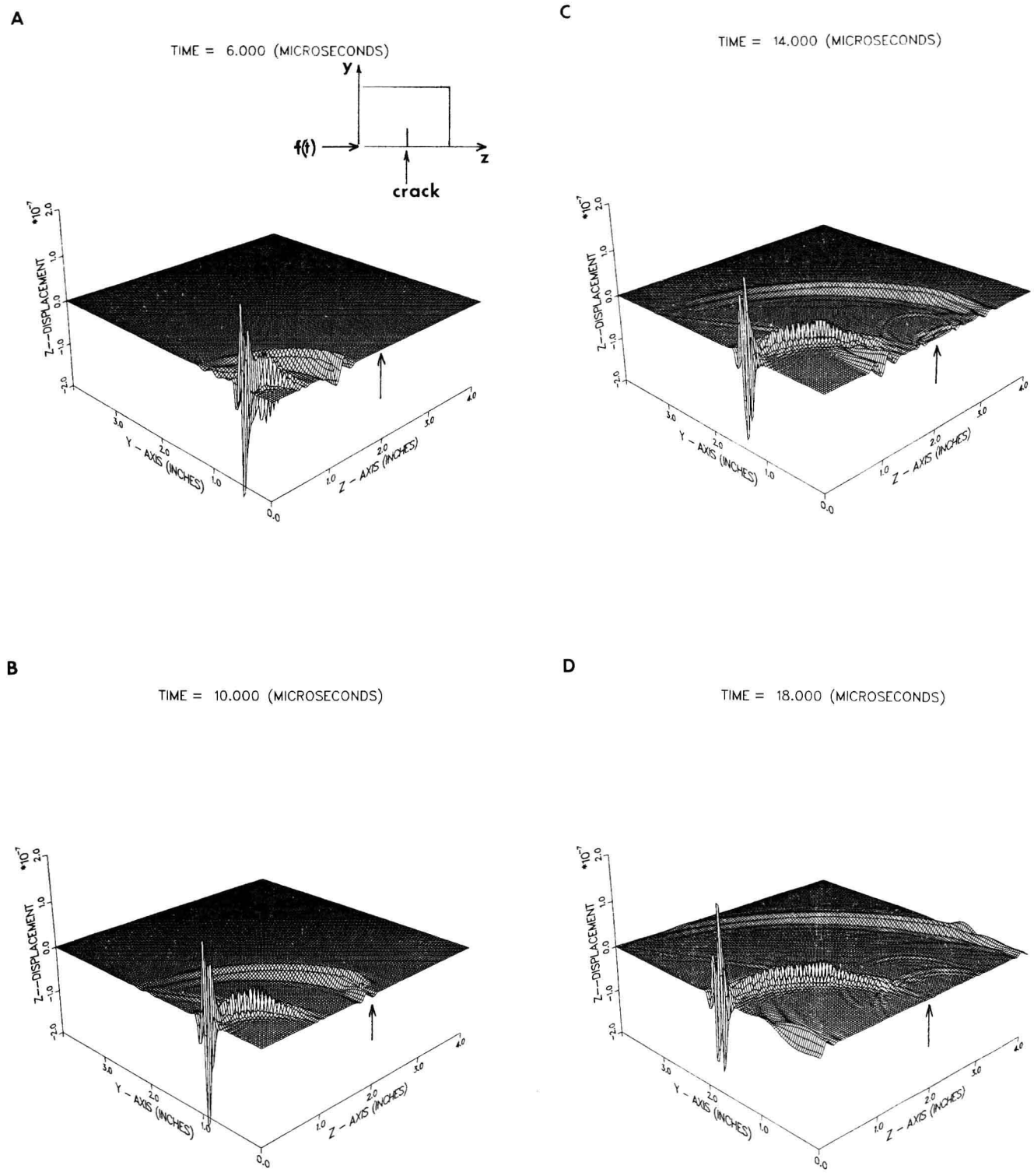

Fig. 2. Bulk wave interactions with a subsurface tight crack.

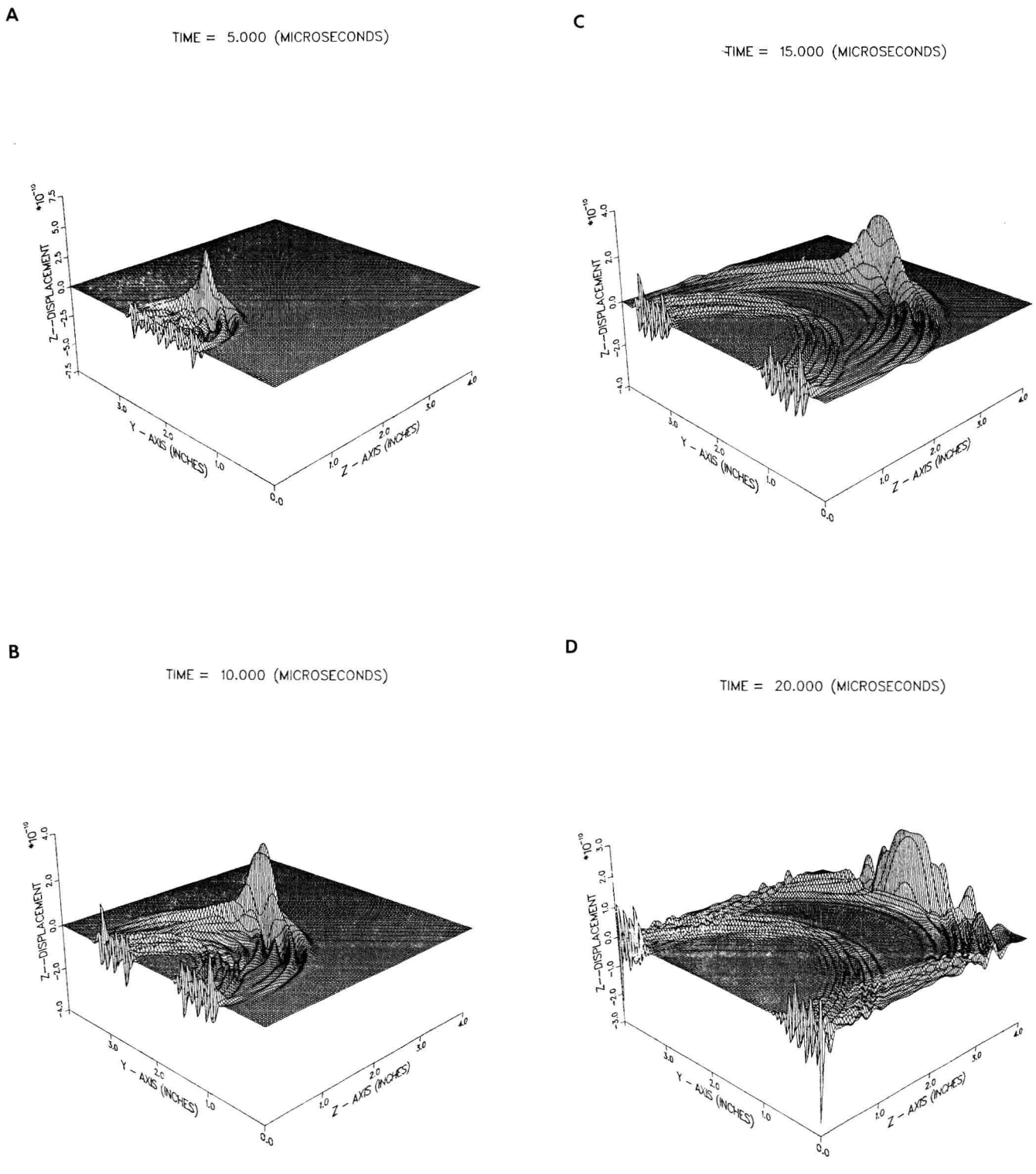

Fig. 3. Wave propagation from a finite aperture transducer in an orthorhombic material parallel to the grain axis.

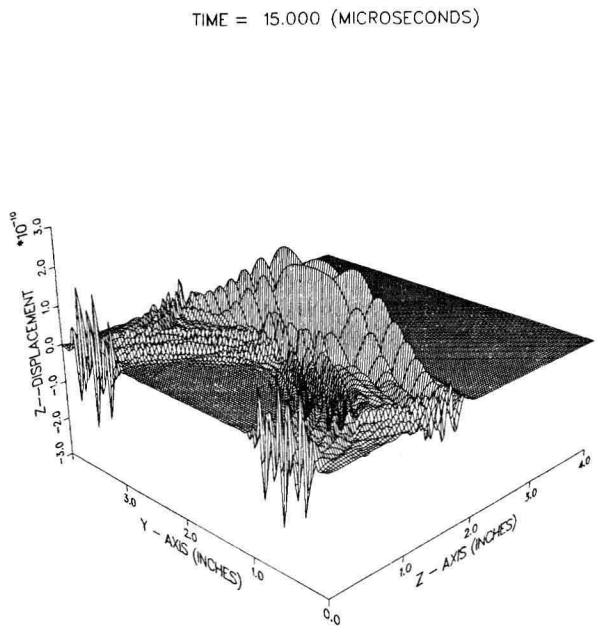

Fig. 4. Wave propagation from a finite aperture transducer in an orthorhombic material perpendicular to the grain axis.

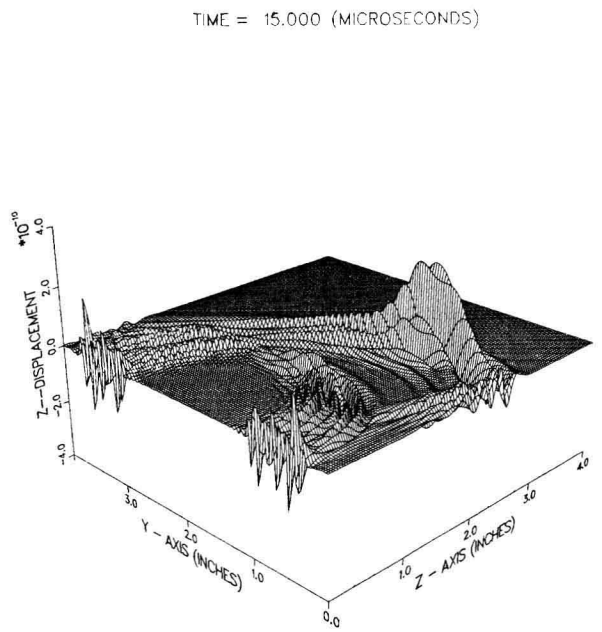

Fig. 5. Wave propagation from a finite aperture transducer in an orthorhombic material at an angle of 45° to the grain axis.

Demerdash, N.A., and Nehl, T.W., 1979, "An Evaluation of the Methods of Finite Elements and Finite Differences in the Solution of Nonlinear Electromagnetic Fields in Electrical Machines," IEEE Transactions on Power Apparatus and Systems, Vol. 98, pp. 74-87.

Harumi, K.F. Suzuki, and Y. Saito, 1973, "Computer Simulation of Nearfield for Elastic Waves in A solid Half-Space," Journal of the Acoustical Society of America, Vol. 53, p. 60.

Hwang, J.H., and Lord, W., 1975, "Finite Element Modeling of Magnetic Field/Defect Interactions," ASTM Journal of Testing and Evaluation, Vol. 3, No. 1, pp. 21-25.

Ida, N., and Lord, W., 1983, "3-D Finite Element Prediction of Magnetostatic Leakage Fields, "IEEE Transactions on Magnetics, Vol. MAG-19, No. 5, pp. 2260-2265.

Ida, N., Palanisamy, R., and Lord, W., 1983, "Eddy Current Probe Design Using Finite Element Analysis," Materials Evaluation Vol. 41, No. 12, pp. 1389-1394.

Ida, N., and Lord, W., 1985, "3-D Finite Element Modeling of Eddy Current NDT Phenomena", IEEE Transactions on Magnetics, Vol. MAG-21, No. 6, pp. 2635-2643.

Ida, N., Hoshikawa, H., and Lord, W., 1985, "Finite Element Prediction of Differential EC Probe Signals from Fe_3O_4 Deposits in PWR Steam Generators", NDT International, Vol. 18, No. 6, pp. 331-338.

Lord, W., and Palanisamy, R., 1981, Development of Theoretical Models for NDT Eddy Current Phenomena, in Eddy Current Characterization of Materials and Structures, ASTM STP 722, G.B. Birnbaum and G. Free, Eds., ASTM, pp. 5-21.

Lord, W., 1983, "Applications of Numerical Field Modeling to Electromagnetic Methods of Nondestructive Testing", IEEE Transactions on Magnetics, Vol. MAG-19, No. 6, pp. 2437-2442.

Lord, W., Palanisamy, R., and Satish, S.S., 1983, "Electromagnetic Methods of Detecting Magnetite in PWR Steam Generators", ASM Journal of Materials for Energy Systems, Vol. 5, No. 2, pp. 112-116.

Lord, W., 1987, "Eddy Current Methods of Flaw Detection and Their Modeling", in Electromagneto-Mechanical Interactions in Deformable Solids and Structures, Y. Yamamoto and K. Miya, Eds., North Holland, pp. 203-213.

Lord, W., Sun, Y.S., Udpa, S.S., and Nath, S., 1988, "A Finite Element Study of the Remote Field Eddy Current Phenomenon", IEEE Transactions on Magnetics, Vol. MAG-24, No. 1, pp. 435-438.

Ludwig, R., Moore, D., and Lord, W., 1987, "Transducer Models for the Finite Element Simulation of Ultrasonic NDT Phenomena", in Review of Progress in Quantitative NDE, D.O. Thompson and D.E. Chimenti, Eds., Plenum Press, Vol. 6A, pp. 649-655.

Ludwig, R., and Lord, W., 1988a), "A Finite Element Study of Ultrasonic Wave Propagation and Scattering in an Aluminum Block", Materials Evaluation, vol. 46, No. 1, pp. 108-113.

Ludwig, R., and Lord, W., 1988b), "A Finite Element formulation for the Study of Ultrasonic NDT Systems", to be published in the IEEE Transactions on Ultrasonics, Ferroelectrics, and Frequency Control.

Ludwig, R., Moore, D., and Lord, W., 1989, "An Analytical and Numerical Study of Transient Force Excitations on an Elastic Half-Space", submitted for publication in the IEEE Transactions on Ultrasonics, Ferroelectrics, and Frequency Control.

Palanisamy, R., and Lord, W., 1980a), "Detection and Modeling Magnetite Buildup in Steam Generators", IEEE Transactions on Magnetics, Vol. MAG-16, No. 5, pp. 695-697.

Palanisamy, R., and Lord, W., 1980b), "Finite Element Analysis of Eddy Current Phenomena", Materials Evaluation, Vol. 38, No. 10 pp. 39-43.

Silvester, P., and Chari, M.V.K., 1970, "Finite Element Solution of Saturable Magnetic Field problems," IEEE Transactions on Power Apparatus and Systems, vol. 89, pp. 1642-1651.

Udpa, S.S., and Lord, W., 1984, "A Fourier Descriptor Classification Scheme for Differential Probe Signals", Materials Evaluation, Vol. 42, No. 9, pp. 1136-1141.

Zienkiewicz, O.C., 1977, The Finite Element Method, McGraw-Hill.

OBSERVABLES DUE TO BEAM-TO-MODE CONVERSION OF A HIGH FREQUENCY GAUSSIAN P-WAVE INPUT IN AN ALUMINUM PLATE IN VACUUM

I. T. Lu and L. B. Felsen
Department of Electrical Engineering and Computer Science

J. M. Klosner
Department of Mechanical and Industrial Engineering

Polytechnic University
Farmingdale, New York

I. INTRODUCTION

Identification of flaws in solid or laminated materials by ultrasound requires detailed knowledge of the excitation, propagation, scattering and detection of high frequency sound waves in the flawed environment. Based on an understanding of these fundamental wave phenomena, one may then attempt to construct an analytical model, with an accompanying algorithm, so as to parametrize the NDE problem in terms of "good observables". For example, a good parametrization for an elongated debonding flaw, which reacts primarily to tangential shear but not to compressional excitation, would involve an input tuned to maximizing shear at the flaw site, and a detector tuned to receiving the shear-excited scattered field. For narrow band signals, beam-type transducers and receivers can furnish the spatial spectral resolution required to achieve such selectivity. Within these perspectives, the present study is directed toward clarifying the wave phenomena that accompany a Gaussian beam input into a layered elastic environment as exemplified (though the general multilayer theory has been developed) by an aluminum plate in vacuum. The Gaussian input has been chosen because a) Gaussians are good models for smoothly tapered outputs from actual transducers, and b) they can be used as discrete basis elements on a (configuration)-(spatial wavenumber) phase space lattice to model rigorously *any* transducer output (1). The Gaussian input is analyzed via the complex source point (CSP) method, by which beam excitation solutions in any (here, the layered) environment are obtained from line or point source excitation solutions in that environment by assigning complex values to the source coordinate location (2, 3). This avoids the need for spatial spectral decomposition of the beam field, as is customary. Previous applications of the CSP method, which requires careful study of the analytic continuation to the complex source domain, have not dealt with elastic layers. Some difficulties encountered in this process are still under investigation, but in the application here to a compressional (P) beam input, they are de-emphasized and do not affect the validity of the results.

Source-excited high frequency propagation in layered advanced materials can be analyzed by ray field tracing, modal expansion and, most generally, by a self-consistent hybrid ray-mode scheme (4). In the hybrid combination, the rays and modes (or wavefronts and resonances under transient conditions) are complementary in the sense that, via a bilateral equivalence, cumulative effects in the one can be expressed as sparse effects in the other. This can form the basis for a good parametrization of wave propagation and scattering processes in flawed layered configurations. The ray-mode equivalence and the hybrid scheme have been formalized in earlier publications (4, 5). Test calculations, especially under transient excitation, have confirmed that these wave types are indeed observed in the signal response and therefore can be classified as good observables (6).

The CSP substitution extends these formulations to beam excitation. Due to P-SV coupling at the plate boundaries, an initially well collimated P beam becomes diffuse and, after a few reflections, is no longer resolvable, therefore ceasing to be a good observable. The field in the plate rapidly assumes more of a mode-like behavior, with a special role assigned to those modes whose constituent plane wave spectra line up closest with those of the incident beam. Special attention is paid to the transitional process, with emphasis on any discernible features in the total fields that could be employed to parametrize flaw excitation and detection when these fields interact with a fault zone. This necessitates careful examination of numerical data (developed here by the CSP-extended mode formulation, with independent checks via the beam tracing formulation), both in the plate cross sections that would encompass a flaw, and along the surface where the detectors would be placed. Typical examples for near, intermediate and far zone observations have been selected from extensive numerical tests, and are presented in the form of the compressional and shear potentials, and the associated horizontal and vertical displacements. Depending on such parameters as beam width, incident beam angle, etc., discernible features in the data are identified, which could lead to a good parametrization of a flawed environment sensitive to horizontal shear.

In Section II, we summarize the hybrid ray-mode method for a line forcing function exciting an elastic plate, and then discuss in Section III how the response to a beam input can be derived therefrom by the complex source coordinate substitution. Certain difficulties are noted in this context, some of which are still under investigation. The numerical results in Section IV for the beam-excited P and SV potentials, as well as the corresponding stresses and displacements, are prefaced by analytical estimates that anticipate conditions where prominent wave phenomena can be well resolved and therefore qualify as good observables in the desired parametrization. These considerations are then tested on the numerical data with a view toward interpreting what is observed. The conclusions in Section V seek to relate what has been done to the next phase that includes a weak debonding flaw in an otherwise perfectly bonded layered composite (7).

II. LINE SOURCE EXCITATION OF AN ELASTIC PLATE

A. Formulation and Solution

An elastic plate with thickness a, characterized by Lamé constants λ and μ and by density ρ, is assumed to be excited by a line source at $x=x'$, $z=z'$ as shown in Fig. 1a. The fields in this plate can be derived from two potentials Φ and Ψ representing pressure and vertically polarized shear waves with respective propagation speeds $v_p = [(\lambda + 2\mu)/\rho]^{1/2}$ and $v_s=[\mu/\rho]^{1/2}$. If the line source excites only time-harmonic compressional (P) waves, the relevant potential problems (with suppressed time dependence $\exp(-i\omega t)$) are defined by the wave equations

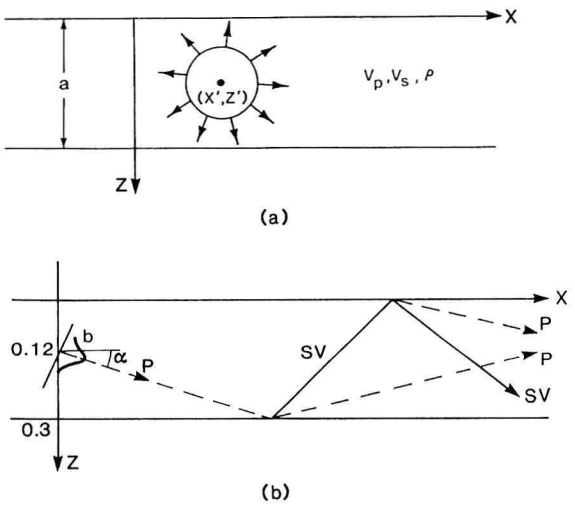

Fig. 1 Elastic plate with thickness a, characterized by wave velocities v_p, v_s and by density ρ.

(a) real source coordinates (x', z') (P-wave isotropic line source).

(b) complex source coordinates $(\tilde{x}', \tilde{z}')$ (P-wave beam source). The beam parameter b in Eq. (18) is related to the (1/e) beam width w_e at the waist by $w_e=(2b/k_p)^{1/2}$. Also shown on this figure are the axes of the incident and reflected P-beams (dashed lines), and of the coupled SV-beams (solid lines), and their relationship to the cross sections in Fig. 2.

$$\left[\frac{\partial^2}{\partial x^2}+\frac{\partial^2}{\partial z^2}+k_p^2\right]\Phi(x,x',z,z')=-\delta(x-x')\delta(z-z'),\ k_p=\omega/v_p$$

$$\left[\frac{\partial^2}{\partial x^2}+\frac{\partial^2}{\partial z^2}+k_s^2\right]\Psi(x,x',z,z')=0, k_s=\omega/v_s \quad (1)$$

In terms of these potentials, the stress components on a plane z = const., subject to free stress boundary conditions at z = 0 and z = a, are

$$\tau_{xz}=\mu\left[2\frac{\partial^2}{\partial x\partial z}\Phi+\left(\frac{\partial^2}{\partial x^2}-\frac{\partial^2}{\partial z^2}\right)\Psi\right]$$

$$\sigma_z=\lambda\left(\frac{\partial^2}{\partial x^2}+\frac{\partial^2}{\partial z^2}\right)\Phi+2\mu\left(\frac{\partial^2}{\partial z^2}\Phi+\frac{\partial^2}{\partial x\partial z}\Psi\right) \quad (2)$$

and the x and z displacements are

$$u_x=\frac{\partial\Phi}{\partial x}-\frac{\partial\Psi}{\partial z}$$

$$u_z=\frac{\partial\Psi}{\partial x}+\frac{\partial\Phi}{\partial z} \quad (3)$$

A plane wave spectral representation of the potentials can be obtained by applying a Fourier transform along the x coordinate,

$$\hat{V}(k;z,z')=\int_{-\infty}^{\infty} V(x,x';z,z')\exp[-ik(x-x')]d(x-x')$$

with the inverse

$$V(x,x',z,z')=\frac{1}{2\pi}\int_{-\infty}^{\infty}\hat{V}(k;z,z')\exp[ik(x-x')]dk \quad (4)$$

where V and $\hat{V}$ are wave vectors in the configuration and spectral domains, respectively,

$$V=\begin{bmatrix}\Phi\\ \Psi\end{bmatrix},\ \hat{V}=\begin{bmatrix}\hat{\Phi}\\ \hat{\Psi}\end{bmatrix} \quad (5)$$

A systematic procedure of solving for the z-dependent amplitudes corresponding to a given spectral wavenumber k in the x-domain has been presented previously (8), and the relevant formulas are summarized below. It is convenient to introduce the propagator matrix

$$\underset{\sim}{E}(d)=\begin{bmatrix}\exp(i\kappa_p d) & 0\\ 0 & \exp(i\kappa_s d)\end{bmatrix} \quad (6)$$

the source vector

$$S=\begin{bmatrix}\frac{-1}{2i\kappa_p}\\ 0\end{bmatrix} \quad (7)$$

and the reflection matrices at the upper and lower boundaries

$$\underset{\sim}{\Gamma}^{U,D}=\begin{bmatrix}\Gamma_{pp} & \pm\Gamma_{ps}\\ \pm\Gamma_{sp} & \Gamma_{ss}\end{bmatrix} \quad (8)$$

with Γ_{ij}, $\{ij\} = \{ps\}$, representing the reflection coefficient into wave i due to an incident wave j,

$$\Gamma_{pp}=\Gamma_{ss}=[4k^2\kappa_p\kappa_s-(\kappa_s^2-k^2)^2]\cdot\Delta_\gamma^{-1},\ \Delta_\gamma=4k^2\kappa_p\kappa_s+(\kappa_s^2-k^2)^2$$

$$\Gamma_{ps}=4(\kappa_s^2-k^2)k\kappa_s\cdot\Delta_\gamma^{-1},\ \Gamma_{sp}=-4(\kappa_s^2-k^2)k\kappa_p\cdot\Delta_\gamma^{-1} \quad (9)$$

In these equations, κ_p and κ_s are transverse wavenumbers for the P- and SV-waves, respectively,

$$\kappa_p=\sqrt{k_p^2 - k^2},\quad \kappa_s=\sqrt{k_s^2 - k^2},\quad \mathrm{Im}(\kappa_{p,s})\geq 0 \qquad (10)$$

To explore the wave phenomena in broad generality, it is necessary to decompose the full spectral amplitude vector into the four categories $\hat{V}^{(\ell)}$, $\ell = 1, 2, 3, 4$ (see Fig. 2),

$$\hat{V}(k,z,z')=\sum_{\ell=1}^{4}\hat{V}^{(\ell)}(k;z,z') \qquad (11)$$

each of which can be expressed as,

$$\hat{V}^{(\ell)}=(\underset{\sim}{I}-\underset{\sim}{F}^{(\ell)})^{-1}\cdot\underset{\sim}{T}^{(\ell)}\cdot S+\Delta^{(\ell)} \qquad (11a)$$

where $\underset{\sim}{I}$ is the identity matrix. The translation matrices connecting the levels z and z′ are

$$\underset{\sim}{T}(\ell) = \begin{cases} \underset{\sim}{E}(a-z)\cdot\Gamma^{D}\cdot\underset{\sim}{E}(a-z') & , \ \ell = 1 \\ \underset{\sim}{E}(z-z') & , \ \ell = 2 \\ \underset{\sim}{E}(z)\cdot\underset{\sim}{\Gamma}^{U}\cdot\underset{\sim}{E}(z') & , \ \ell = 3 \\ \underset{\sim}{E}[-(z-z')] & , \ \ell = 4 \end{cases} \qquad (11b)$$

and the reverberation matrices are

$$\underset{\sim}{F}^{(\ell)}(k,z)=\begin{cases} \underset{\sim}{E}(z)\cdot\underset{\sim}{\Gamma}^{U}\cdot\underset{\sim}{E}(a)\cdot\Gamma^{D}\cdot\underset{\sim}{E}(a-z), & \ell = 1,2 \\ \underset{\sim}{E}(a-z)\cdot\underset{\sim}{\Gamma}^{D}\cdot\underset{\sim}{E}(a)\cdot\underset{\sim}{\Gamma}^{U}\cdot\underset{\sim}{E}(z), & \ell = 3,4 \end{cases} \qquad (11c)$$

Finally, $\Delta^{(\ell)}$ represents vectors that remove the direct ray where it does not exist in the respective category,

$$\Delta^{(\ell)}=\begin{cases} 0 & \ell = 1,3 \\ -U[-(z-z')]\underset{\sim}{E}(z-z')\cdot S, & \ell = 2 \\ -U(z-z')\underset{\sim}{E}[-(z-z')]\cdot S, & \ell = 4 \end{cases}$$

$$U(\bar{z})=\begin{cases} 1 & \bar{z}>0 \\ 1/2 & \bar{z}=0 \\ 0 & \bar{z}<0. \end{cases} \qquad (11d)$$

As mentioned already, the derivation of these results may be found in (8).

B. Alternative Representations

From the basic closed form solution in (11a), it is possible to derive a variety of alternative representations with different physical content. These alternatives, discussed in detail in (7), are likewise summarized here. For convenience, the superscript "ℓ" for the ℓ^{th} category is omitted in what follows.

1. Modal Expansion A representation in terms of the x-guided normal modes V_m in the plate is developed by evaluating the spectral integral in (4) around the pole singularities which define the modal resonances (eigenvalues) k_m. The resonance equation for the modal poles

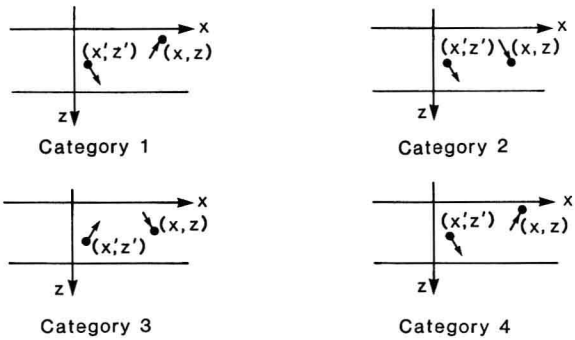

Fig. 2 The four categories that order the propagation process according to waves which are upgoing or downgoing, respectively, with respect to the source depth z′ and arrive at z from an upward or downward direction.

$k = k_m$, $m = 1, 2...$, is given by

$$\det(\underset{\sim}{I}-\underset{\sim}{F}) = \{1-(\exp[i(\kappa_p+\kappa_s)a])^2\} - \Gamma_{pp}^2[\exp(i\kappa_p a) - \exp(i\kappa_s a)]^2 = 0 \qquad (12)$$

which leads to the corresponding mode series

$$V = \sum_m V_m \qquad (13)$$

with the modal coefficients

$$V_m = i \lim_{k\to k_m}[(k-k_m)\hat{V}\exp(ik(x-x'))] \qquad (13a)$$

Because of the stress-free boundary conditions at z = 0, a, the mode spectrum is purely discrete.

2. Ray Expansion A representation in terms of generalized ray integrals V_n results from expanding the resonance producing matrix in a power series

$$(\underset{\sim}{I}-\underset{\sim}{F})^{-1}=\sum_{n=0}^{\infty}\underset{\sim}{F}^{n} \qquad (14)$$

and substituting into (11), (11a), and (4) to obtain

$$V=\sum_{n=0}^{\infty}V_n,\quad V_n=\frac{1}{2\pi}\int_{-\infty}^{\infty}\underset{\sim}{F}^{n}\cdot\underset{\sim}{T}\cdot Se^{ik(x-x')}\,dk \qquad (15)$$

The index n can be regarded as an ordering parameter counting the number of generalized ray reverberations.

3. Hybrid Ray–Mode Representation A hybrid form combining modes and generalized rays results from partial series expansion of the resonance producing matrix,

$$(\underset{\sim}{I}-\underset{\sim}{F})^{-1}=\sum_{n=0}^{N-1}\underset{\sim}{F}^{n}+(\underset{\sim}{I}-\underset{\sim}{F})^{-1}\cdot\underset{\sim}{F}^{N} \qquad (16)$$

which, upon substitution into (11) with (11a), yields a finite sum of ray integrals and a remainder integral. The remainder integral can be reduced by deforming the integration path from the real axis in the complex k-plane, whereon the integrand is highly oscillatory, into a (steepest descent type) contour C_N whereon the integrand decays rapidly away from a central region. Pole singularities intercepted during the path deformation furnish normal modes whose number is determined *uniquely* by the ray index N and the location of the

deformed contour. The resulting hybrid ray-mode representation has the form,

$$V = \sum_{n=0}^{N-1} V_n + \sum_{m} V_m + R_N \qquad (17)$$

where

$$R_N = \frac{1}{2\pi} \int_{C_N} (\underset{\sim}{I} - \underset{\sim}{F})^{-1} \cdot \underset{\sim}{F}^N \cdot \underset{\sim}{T} \cdot S e^{ik(x-x')} dk \qquad (17a)$$

is the modified remainder with more favorable convergence properties than the real-k remainder integral.

III. BEAM EXCITATION OF AN ELASTIC PLATE

To convert the wave fields generated by the P-wave isotropic line source treated in Section II (Fig. 1a) into wave fields corresponding to excitation by a P- wave Gaussian beam source (Fig. 1b), we shall employ the complex source point technique mentioned earlier. This requires analytic continuation of all wavefield expressions from the real source coordinates (x', z') to the complex source coordinates

$$\tilde{x}' = x' + ib\cos\alpha, \quad \tilde{z}' = z' + ib\sin\alpha \qquad (18)$$

where (x',z') now locates the center of the beam waist, b is a beam width parameter, and α is the angle between the beam axis and the positive x-axis (see Fig. 1b and (2, 3). While the analytic extension guarantees *formally* that the resulting P and SV potentials satisfy the appropriate wave equations and boundary conditions, the validity of a particular wavefield *representation* must be verified in each case; i.e., the representation obtained on replacing (x',z') by $(\tilde{x}', \tilde{z}')$ must remain convergent. It turns out that various alternative representations require different continuation strategies. These aspects have been considered in (8), and salient features are summarized below.

When the wavefield representation is in the form of a spectral integral over the spatial wavenumber k corresponding to the x-coordinate as in (4) or (15), the analytic extension can be carried out systematically by contour deformation, if required for convergence (3). For the multiply reflected beam integrals derived from the generalized ray integrals in (15), convergence can be stabilized by switching from the global (x, z) coordinates to the *local* coordinates defined with respect to the axes of the individual beams (see Fig. 3). This transformation avoids problems arising from strongly oblique spectra with respect to the beam axes, corresponding to nearly horizontal beam propagation referred to a fixed x- coordinate frame. It also de-emphasizes problems attributable to boundary-reflection-induced P-SV coupling of evanescent P spectra in the x-referred spectral interval $k_p < k < k_s$, wherein the SV spectra are still propagating (9).

The same spectral interval is troublesome when the field representation is in the form of a series like the normal mode or the hybrid ray-mode expansions in (13) or (17), which are tied to the global (x, z) system. Contour deformation is now not an immediately available option, and direct complex source coordinate $(x', \tilde{z}')$ substitution may cause convergence problems due to exponentially growing factors in the series elements generated by the evanescent spectra. Since these effects are nonphysical because the source beam spectrum in the interval $k_p<k<k_s$ is decaying, we have for the present simply ignored the modes with modal eigenvalues $k_m>k_p$ because their excitation strength by the P-wave source is minimal. Numerical comparisons with fields computed by the beam tracking algorithm have confirmed the validity of this assumption. It may be noted that these difficulties are not encountered with an SV beam input because the source spectrum then spans the totality of propagating waves $k<k_s$.

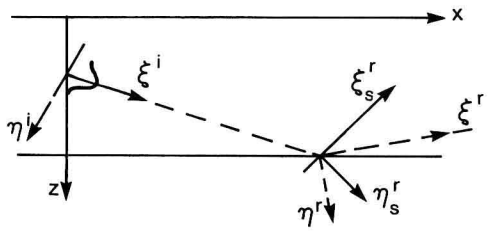

Fig. 3 Local coordinates (ξ,η) defined with respect to the axes of the individual beams. (ξ^i,η^i)= incident P-beam; (ξ^r,η^r)= reflected P-beam; (ξ^r_s,η^r_s)= reflected SV-beam.

IV. NUMERICAL RESULTS

Extensive numerical computations have been performed to chart the evolution of the P-beam input as it interacts successively with the plate boundaries and undergoes P-SV coupling at each reflection. The results have been generated by the analytically continued mode series in (13), subject to the above-noted omission of modes with eigenvalues $k_m>k_p$. Spot checks performed by the multiple reflected beam algorithm derived from (15) by complex source coordinate substitution and stabilized around the local beam coordinates have established that this assumption is valid. The hybrid beam-mode format corresponding to (17) has not yet been implemented numerically but the results to be discussed below strongly suggest that such a description is worthy of consideration because the physical observables clearly appear beam-like in certain parametric domains and mode-like in others. It is possible to anticipate certain distinctive features that are desirable for a good parametrization by looking at the P and SV potentials individually, interpreting these, and drawing possible inferences therefrom for the physically observed horizontal and vertical displacements in the plate cross sections and on the surfaces, which are generated by interfering contributions from both wave species. These considerations have been discussed in (7) and they have guided the choice of examples to follow. The individual potentials are informative for displacements when one is dominant over the other. Except when noted otherwise, the plate and beam parameters (see Fig. 1) used in the examples are those listed in the caption for Fig. 4.

All numerical computations were performed on a PC/AT compatible Everex 10 MHz System 1800, having a fast 10 MHz 80287 math coprocessor. The potentials were calculated by the normal mode expansion in (13); for near zone observational domains covered by a workable number of beam reflections, they were also calculated by the beam series in (15). Both procedures have been found to yield the same numerical values. In the normal mode expansion, we have retained only those modes (64 in this example) with $k_m<k_p$ because the incident P-beam couples very weakly to the troublesome evanescent P spectra contained in modes $k_m>k_p$. In all cases, the normal mode expansion was used as the reference solution.

Results are shown for an incident P-beam with beam-axis inclination α=31.4° and 71.8°. The axes of the incident P-beam (dashed), the reflected P-beams (dashed), and the converted SV-beams (solid) are indi-